Supporting Information

Highly Monodispersed PbS Quantum Dots for Outstanding Cascaded-Junction Solar Cells

Bo Hou,[†] Yuljae Cho,[†] Byung Sung Kim,[†] John Hong,[†] Jong Bae Park,[‡] Se Jin Ahn,[Δ] Jung Inn Sohn,[†] SeungNam Cha,[†]* Jong Min Kim[§]*

†. Department of Engineering Science, University of Oxford, Parks Road, Oxford OX1 3PJ, UK http://www.eng.ox.ac.uk/nst

‡. Jeonju centre, Korea Basic Science Institute, Jeonju, Jeollabuk-do 54907, Republic of Korea

Δ. New and Renewable Energy Research Division, Photovoltaic Laboratory, Korea Institute of Energy Research (KIER), 152 Gajeong-ro, Yuseong-gu, Daejeon 305-343, Republic of Korea

§. Department of Engineering, University of Cambridge, 9 JJ Thomson Avenue, Cambridge CB3 0FA, UK

SI. Sample preparation methods:

Chemicals.

Lead (II) oxide (PbO, 99.999% trace metals basis), hexamethyldisilathiane (bis (trimethylsilyl) sulphide, TMS, synthesis grade), tetrabutylammonium iodide (TBAI, reagent grade, 98%), 1,2-ethanedithiol (EDT, technical grade, ≥90%), 1-octadecene (ODE, technical grade, 90%), oleic acid (technical grade, OA, 90%), methanol (ACS reagent, ≥99.8%), acetone (CHROMASOLV®, for HPLC, ≥99.8%), ethanol (for HPLC, gradient grade, ≥99.8%), toluene (anhydrous, 99.8%), hexane (CHROMASOLV®, for HPLC, ≥99.8%), zinc acetate dehydrate (ACS reagent, ≥98%), chloroform (anhydrous, ≥99%), butylamine (99.5%) and potassium hydroxide (ACS reagent, KOH, ≥85%) were purchased from Sigma-Aldrich and were used without any further purification.

Synthesis and purification of PbS QDs.

The Pb precursor was prepared in a two-neck flask, which was equipped with 0.47 g (2.106 mmol) of PbO, 1.49 ml (4.212 mmol) of OA (PbO:OA=1:2) and 12.7 ml of octadecene (ODE). The solution was degassed at 100 ℃ in vacuum for two hours until a clear solution was formed. On the other hand, the sulphur precursor was prepared under Ar atmosphere. Briefly, 210 μl of (TMS) was dissolved in 6.4 ml of ODE in vacuum at room temperature for 2 hours, and then the reaction was switched to Ar atmosphere. After the preparation of Pb and S precursors, the Pb precursor system was flushed with Ar and heated to 130 ℃, the sulphur precursor was loaded into a syringe under Ar and the content of the syringe was injected into the Pb reaction flask swiftly. The reaction flask was subsequently left to cool to room temperature by an ice bath, and the total operation after the injection was kept at 20 seconds. The raw reaction solution was purified by adding a mixture of 5 ml of hexane and 25 ml of acetone followed by centrifugation at 8000rpm. Then, the nanocrystals were washed twice by dissolving in hexane and precipitating with ethanol (1/10, v/v). After drying the precipitate, the PbS QDs were finally dispersed into toluene with a weight concentration of 50 mg/ml for device fabrication and characterization.

Synthesis and purification of ZnO nanoparticles (NPs).

Typically, zinc acetate dehydrate (0.9788 g) was dissolved in 42 ml of methanol in a two-neck flask equipped with glass condenser, and the solution was heated to 60 ℃ under air. Potassium hydroxide (KOH, 0.469 g) was dissolved in 22 ml of methanol and added dropwise into the zinc acetate reaction flask over a period of 10 min. The solution turned into opaque solution after the injection and then slowly turned back to a transparent solution. After a total reaction time of 90 min, the reaction solution changed to a cloudy solution. At this point, the heating mantle was switched off and the flask was cooled to room temperature. The ZnO nanocrystals were precipitated by centrifuging at 8000 rpm for 10min and then re-

dispersed in 30 ml of methanol. This purification process was carried out at least twice to remove the unreacted material. Finally, ZnO NPs were dispersed into chloroform with a weight concentration of 50 mg/ml. It should be noted that the addition of a small amount of methanol would help the dispersing of ZnO NPs to chloroform. Furthermore, 100μl of butylamine was also added as a stabilizing ligand for the long-term storage.

Single ε_{gap} QDSC fabrication.

Patterned ITO substrates were ultrasonically cleaned with acetone, ethanol, and 2-isopropanol subsequently. After the nitrogen blowing, the dried ITO substrates were treated with oxygen plasma for 5min. ZnO layers were fabricated by spin coating a solution of ZnO nanoparticles (50mg/ml) onto ITO substrates at 2000rpm for 30 seconds. Then the ZnO films were annealed at 250 ^{o}C for 10 min on a hot plate under ambient and naturally cooled down to room temperature. PbS QD layers were fabricated through the layer-by-layer spin-casting. For the 1.23 eV PbS QD layer, the PbS solution (50 mg/ml) was spin casted onto the substrate at 2000 rpm for 15 seconds. A TBAI solution (10 mg/ml in methanol) was then applied to the films for 30 seconds, then the films were span at 2000 rpm for 30 seconds, followed by two rinse-spin steps (30 seconds for each step) with methanol. For PbS@EDT layers, an EDT solution (0.02% volume in acetonitrile) was applied to the PbS films by spin casting, following with two rinse-spin steps with acetonitrile (two layers of PbS@EDT should be deposited continually). All the film deposition process was performed under ambient air condition. The devices were stored in air overnight and then transferred to an EDWARD thermal evaporator for the gold electrode evaporation. Gold electrodes were thermally evaporated onto the films through shadow masks. The device areas were defined by applying masks with the area of 0.012 cm^2.

CJQDSC fabrication.

The optimal structure for the CJQDSC consists of 1 layer of 1.03 eV, 10 layers of 1.23 eV and 1 layer of 1.37 eV PbS QDs. The TBAI ligand exchange was applied to 1.03 eV and 1.23 eV PbS QDs, the EDT ligand exchange was applied to 1.37 eV PbS QDs. It should be noted that the two loops of TBAI ligand exchange process is needed for the 1.03 eV PbS QDs in order to remove excess OA ligands from QDs surface. Detail information for the ligand exchange condition as a function of QD ε_{gap} can be found in the supporting information Table S3.

SII. Material characterization methods.

The XRD analysis was carried out using a fully automated Bruker D8 ADVANCE eco powder diffractometer employing copper k_{α} radiation (λ=0.15406 nm) and an LYNXEYE XE detector. The sample was continuously spun during data collection and scanned using a step size of 0.02° (2θ) between the range of 10 °- 90 ° (2θ). The TEM, HRTEM and SAED analysis were performed on a JEOL TEM 2010 and the electron wavelength set at 0.0251 Å. Optical ε_{gap} of as-prepared PbS QDs was analysed by employing a Cary 5000 UV-vis-NIR spectrometer, and the ε_{gap} value was estimated from the wavelength of the first exciton peak. For the UPS measurements, three layers of the PbS QD films with the different ligands (TBAI or EDT) were fabricated using the layer-by-layer spin-coating steps on the ITO substrates. UPS measurements were performed on AXIS – NOVA (KRATOS Inc.) in an ultrahigh vacuum chamber with an incident photon source of He (I) (21.2 eV) discharge lamp and have a resolution of 0.05 eV. The XPS analysis was using a Thermo Scientific K-Alpha XPS instrument equipped with a micro- focussed mono-chromated Al X-ray source. The source was operated at 12 keV and a 400-micron spot size was used. The analyser operated at constant analyser energy (CAE) 200 eV for survey scans and 50eV for detailed scans. Charge neutralization was applied using a combined low energy / ion flood source. The data acquisition and analysis was performed with Thermo Scientifics Avantage software. Peak

fitting (Lorentzian / Gaussian (L/G) 30%) was applied following the removal of a smart background. Normalised atomic percentages were determined from peak areas of the elemental main peaks detected on the survey scan following background subtraction and application of Thermo sensitivity factors. Film thickness is measured by scanning electron microscope (SEM, FEI Quanta 600 FEG) and atomic force microscopy (AFM, Veeco Dimension 3100).

SIII. Device characterization.

The J-V characteristics were recorded using a Keithley 2400 under simulated solar light illumination by a LOT Quantum Design simulator (LSE340/1/850.27C) equipped with a 300 W Xe Arc lamp power supply and an AM 1.5 filter. The light intensity was calibrated with a RERA SOLUTIONS silicon reference cell (RQS4695) before each measurement. By employing a SpeQuest QE system, the external quantum efficiency (EQE) measurement was performed. The QE systems armed with a 100W Quartz Tungsten Halogen light as the photon source, equipped with 150 mm F/4.2 monochromator, an SR830 DSP Lock-In Amplifier (locked to light chopped at 83 Hz) and a Melles Griot IV converter. The wavelength range is from 350 nm to 1100 nm and all the measurement was calibrated by a NIST traceable Silicon (200 nm-1100 nm) reference cell with area pre-defined mask (0.012 cm^2).

SIV: TEM, SAED, HRTEM and XRD analysis of PbS QDs.

In order to analysis the crystal structure (i.e. lattice constant) and morphology (i.e. diameter) of as-prepared PbS QDs. The electron microscopy techniques such as TEM, HRTEM, SAED, and XRD were performed. An systematic powder x-ray diffraction (XRD) analysis of as-prepared PbS QDs in different sizes was also carried out to understand the crystallography evolution during the QD size growth. As shown in the Figure S8a, the rock-salt cubic crystal structure is revealed among the different sizes of the PbS QD (referring to PDF card 78-1057).

Combining the TEM and XRD results, the size of as-prepared PbS QDs can be determined. As shown in the Figure S8b, these statistically plotting results show the relationship of the diameter and ε_{gap} of the PbS QD as a function of OA: PbO mole ratio.

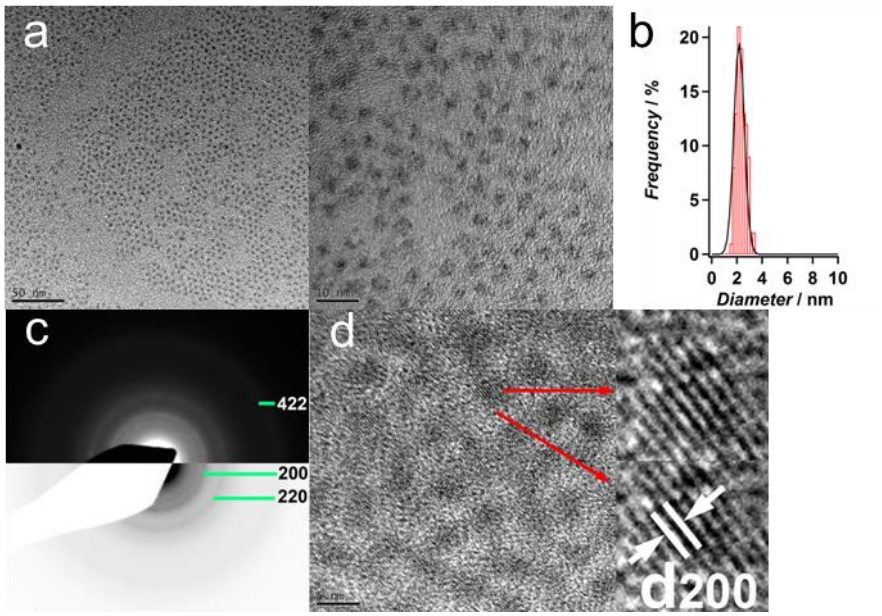

Figure S1 TEM analysis of as-prepared 1.37eV PbS QDs with a size of 2.31±0.4nm and a ratio of OA:PbO=2:1, a) scale bar=50nm left, scale bar=10nm right. b) Sizing histogram of as-prepared PbS QDs with a Gaussian fitting plot peaking at 2.3nm. c) SAED pattern of as-prepared PbS QDs, reflections of {200}, {220} and {422} can be clearly resolved. The average value of lattice constant of cubic PbS calculated from each diffraction is a=6.03±0.04Å. d) A HRTEM image of as-prepared PbS QDs, the lattice distance of (200) plane is analysed as 3.16±0.01Å, which gives a lattice constant of the cubic PbS a=6.32±0.02Å. Scale bar equals to 5nm.

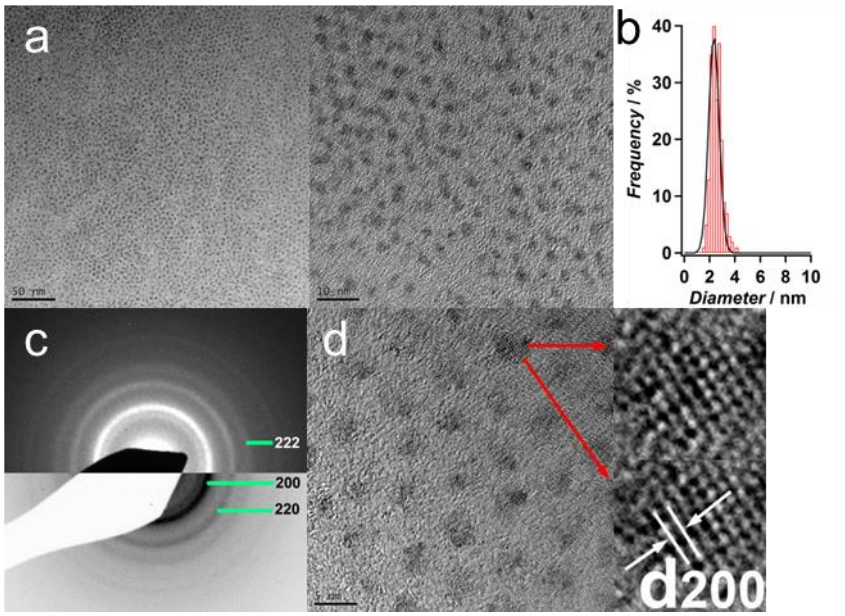

Figure S2 TEM analysis of as-prepared 1.30 eV PbS QDs with a size of 2.48±0.4 nm and a ratio of OA:PbO=3:1, a) scale bar=50 nm left, scale bar=10 nm right. b) Sizing histogram of as-prepared PbS QDs with a Gaussian fitting plot peaking at 2.5 nm. c) The SAED pattern of as-prepared PbS QDs, reflections of {200}, {220} and {222} can be clearly resolved. The average value of lattice constant of cubic PbS calculated from each diffraction is a=5.83±0.05 Å. d) A HRTEM image of as-prepared PbS QDs, lattice distance of (200) plane is analysed as 3.15±0.01 Å, which gives a lattice constant of the cubic PbS a=6.3±0.02 Å. Scale bar equals to 5 nm.

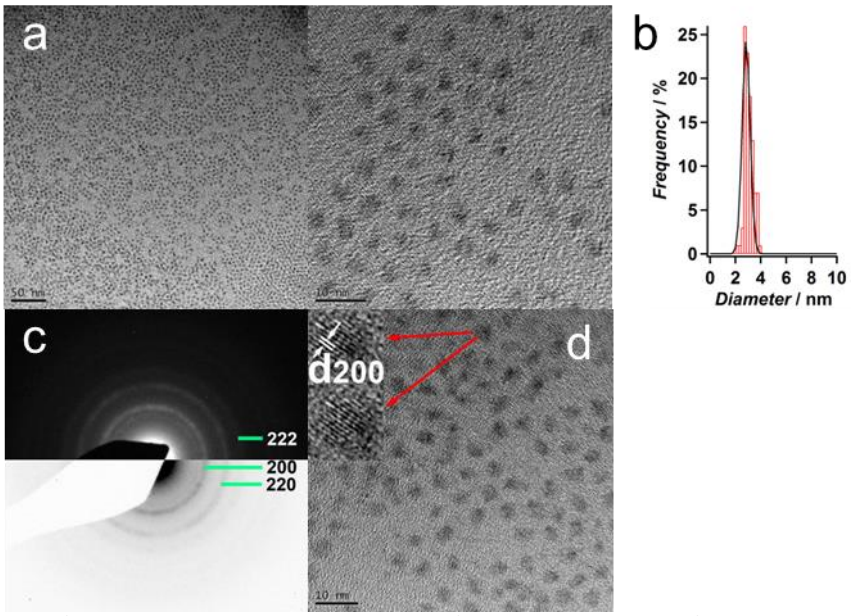

Figure S3 TEM analysis of as-prepared 1.23 eV PbS QDs with a size of 3.01±0.3 nm and a ratio of OA:PbO=5:1, a) scale bar=50 nm left, scale bar=10 nm right. b) Sizing histogram of as-prepared PbS QDs with a Gaussian fitting plot peaking at 3 nm. c) The SAED pattern of as-prepared PbS QDs, reflections of {200}, {220} and {222} can be clearly resolved. The average value of lattice constant of cubic PbS calculated from each diffraction is a=5.62±0.06 Å. d) A HRTEM image of as-prepared PbS QDs, the lattice distance of (200) plane is analysed as 3.15±0.02 Å, which gives a lattice constant of the cubic PbS a=6.3±0.04 Å. Scale bar equals to 10 nm.

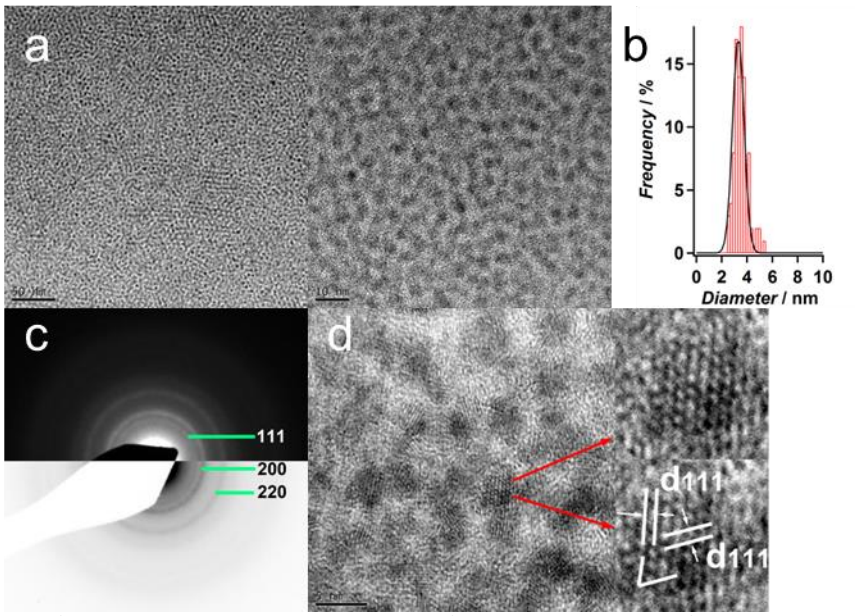

Figure S4 TEM analysis of as-prepared 1.14 eV PbS QDs with a size of 3.48±0.5 nm and a ratio of OA:PbO=8:1, a) scale bar=50 nm left, scale bar=10 nm right. b) Sizing histogram of as-prepared PbS QDs with a Gaussian fitting plot peaking at 3.5 nm. c) The SAED pattern of as-prepared PbS QDs, reflections of {111}, {200} and {220} can be clearly resolved. The average value of lattice constant of cubic PbS calculated from each diffraction is a=5.79±0.05 Å. d) A HRTEM image of as-prepared PbS QDs, lattice distance of (111) plane is analysed as 3.29±0.01 Å, a cross-grating pattern also resolved as indexed, the angle between (111) and (111) planes are measured to be 70.66±0.9 °. A lattice constant of the cubic PbS is calculated to be a=5.7±0.02 Å. Scale bar equals to 5 nm.

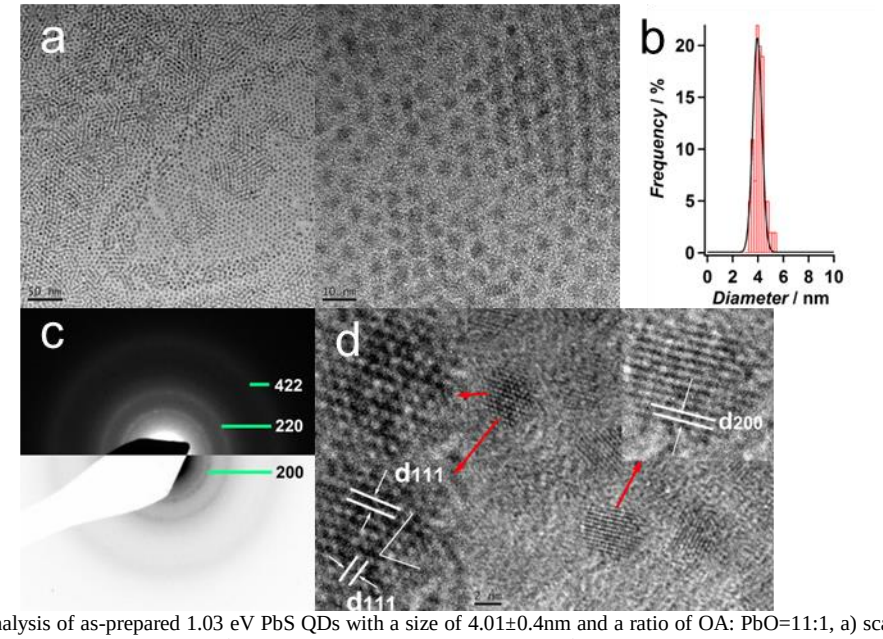

Figure S5 TEM analysis of as-prepared 1.03 eV PbS QDs with a size of 4.01±0.4nm and a ratio of OA: PbO=11:1, a) scale bar=50 nm left, scale bar=10 nm right. b) Sizing histogram of as-prepared PbS QDs with a Gaussian fitting plot peaking at 4 nm. c) The SAED pattern of as-prepared PbS QDs, reflections of {200}, {220} and {422} can be clearly resolved. The average value of lattice constant of cubic PbS calculated from each diffraction is a=6.05±0.04 Å. d) A HRTEM image of as-prepared PbS QDs, lattice distance of (111) plane is analysed as 3.3±0.01 Å and (200) plane is analysed as 2.89±0.04 nm, a cross-grating pattern also resolved as indexed, the angle between (111) and (111) planes are measured to be 70.4±1.5 º. A lattice constant of the cubic PbS is calculated to be a=5.78±0.02 Å. Scale bar equals to 2 nm.

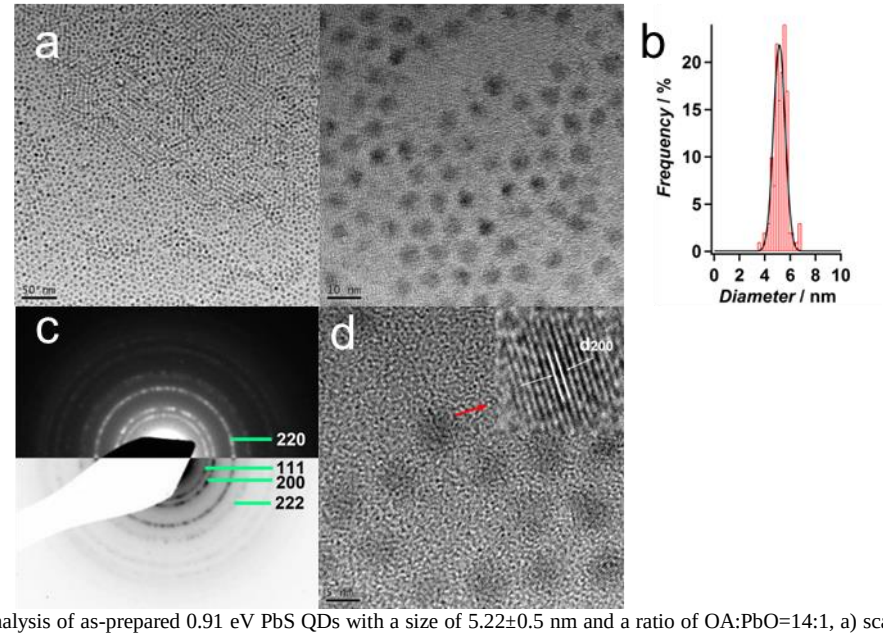

Figure S6 TEM analysis of as-prepared 0.91 eV PbS QDs with a size of 5.22±0.5 nm and a ratio of OA:PbO=14:1, a) scale bar=50 nm left, scale bar=10 nm right. b) Sizing histogram of as-prepared PbS QDs with a Gaussian fitting plot peaking at 5.2 nm. c) The SAED pattern of as-prepared PbS QDs, reflections of {111}, {200}, {220} and {222} can be clearly resolved. The average value of lattice constant of cubic PbS calculated from each diffraction is a=5.85±0.04 Å. d) A HRTEM image of as-prepared PbS QDs, lattice distance of (200) plane is analysed as 2.94±0.01 nm. A lattice constant of the cubic PbS is calculated to be a=5.88±0.02. Scale bar equals to 5 nm.

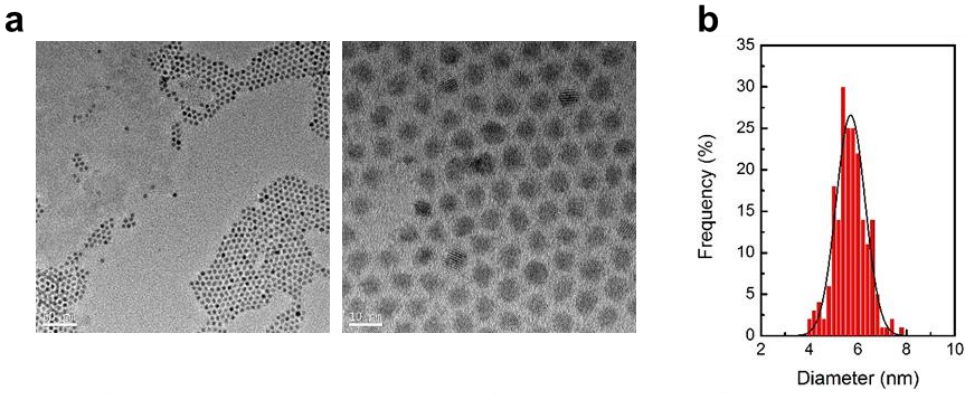

Figure S7 TEM analysis of as-prepared 0.84 eV PbS QDs with a size of 5.8±0.6 nm and a ratio of OA:PbO=14:1. a) Scale bar=50 nm left, scale bar=10 nm right. b) Sizing histogram of as-prepared PbS QDs with a Gaussian fitting plot peaking at 5.8 nm.

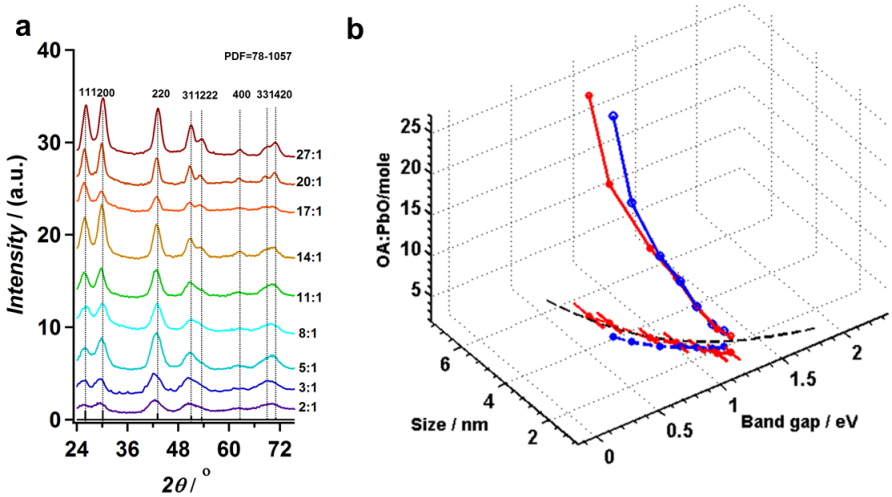

Figure S8 a) XRD patterns of as-prepared PbS QDs with different sizes. The dotted vertical lines are the PbS bulk crystal Bragg angles employed for guiding. The diffraction pattern displayed in a sequence of the precursor mole ratio of oleic acid (OA) to lead (Pb) change from 27:1 to 2:1. b) Plots of QD size and optical ε_{gap} evolution as a function of OA/PbO mole ratio, the size of QD is calculated from theoretical equation (black dashed line), XRD (blue curve) and TEM (red curve). The projection plots on the axes of Size vs. Band gap demonstrate the well consistent between HRTEM, SAED and XRD.

SV: Absorption spectra comparison of two different synthesis approaches and peak to valley ratios extracted from Figure 1b.

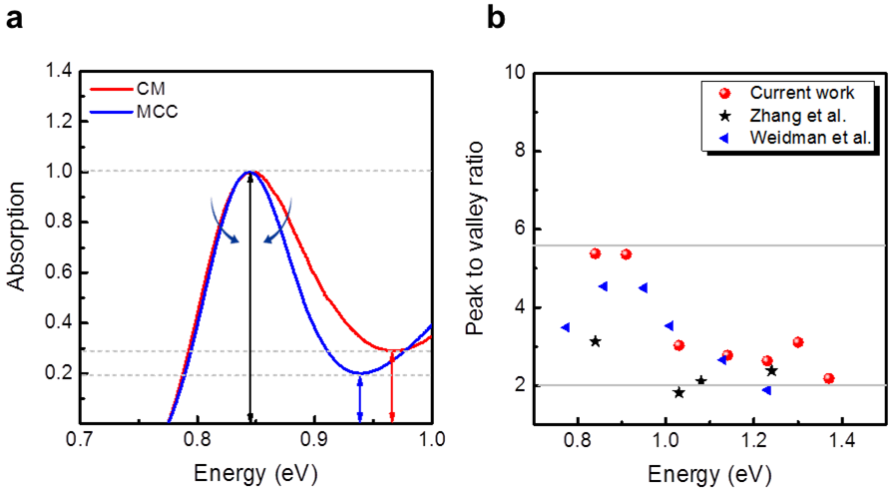

Figure S9. a) Comparison of the first exciton peak of 0.84 eV PbS QDs synthesized from CM method (red curve) and MCC method (blue curve), arrows indicated the narrowing trend between two approaches and peak to valley enhanced from 3.57 to 5.2. b) Peak to valley ratio calculated from absorption spectra (Figure 1b) of different size of as-prepared PbS QDs. Triangle and Pentagram symbols are literature values extracted from two represented references.[1, 2]

SVI: Valence band edge and conduction band edge energy levels calculation from UPS analysis.

The UPS analysis is used to determine the energy levels of Fermi level (ε_ϕ) and the valence band edge (ε_v) of as-prepared ZnO NPs (Figure S10a) and PbS QD films (Figure S10b, e.g. 1.3 eV PbS@TBAI). The reference is equal to the vacuum level. The Fermi level is extracted from the difference between the incident photon energy of 21.2 eV and the high binding energy edge. The energy difference between the ε_v and the ε_f is determined from the low binding energy. The conduction band edge energy level is calculated from the subtraction of the ε_v from the ε_{gap}.

As examined from the UPS shown in Figure S10a, the binding energy of the secondary electron cut-off decrease 130 meV after ZnO thermal annealing, combining a 70 meV decrement in the Fermi edge region, approximately 140meV ε_C downshifting can be identified. As illustrated in Figure S10c, the downshifting of ZnO ε_C increases the band bending between ZnO and PbS QDs layer (i.e. ZnO/PbS@TBAI), which provides an energy barrier that prevents photogenerated electrons (filled circles) from flowing back to the PbS-TBAI layer, it also reduces the surface recombination of photogenerated electrons and holes at the PbS@TBAI layers or TBAI@EDT interface. This electron-extracting layer between the PbS@TBAI layer and the cathode will lead to an improved photocurrent collection efficiency and enhanced device performance.

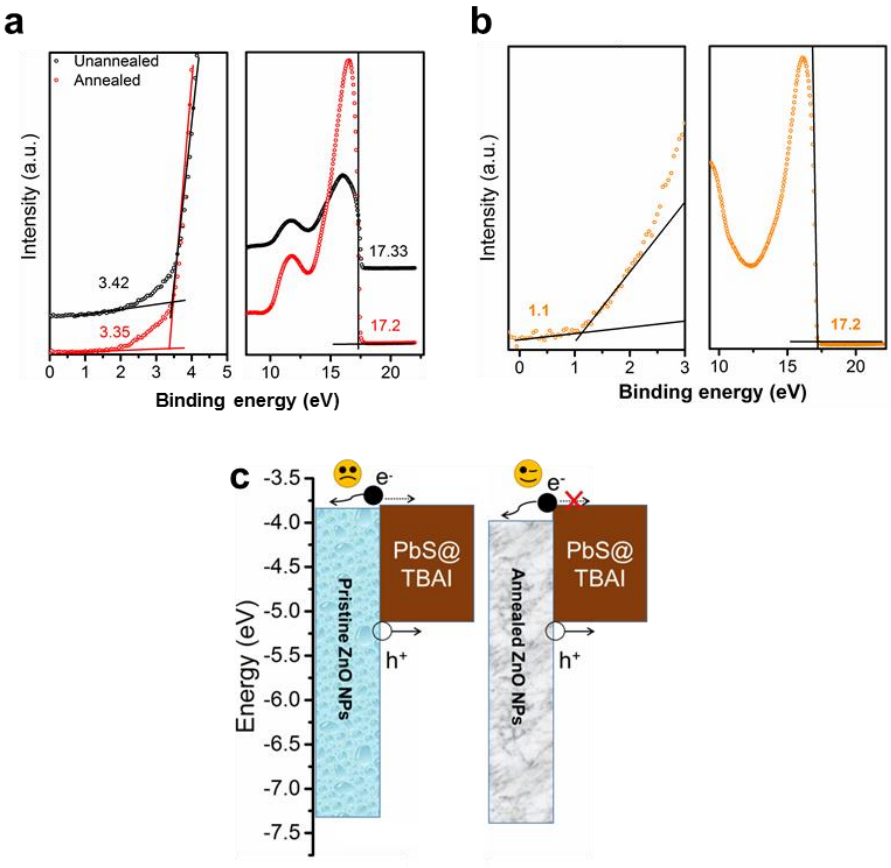

Figure S10 a) UPS spectra of the unannealed ZnO film (black curve) and annealed (red curve) ZnO film. The left panel shows magnified spectra near the Fermi edge and right panel shows the secondary electron cut-off region. Spectra were shifted for clarity. Each ε_{gap} of annealed and pristine ZnO NPs is 3.37 eV and 3.45 eV respectively. b) UPS analysis of the 1.3 eV PbS QD film on the top of ITO slides. The PbS QDs were ligand exchanged by TBAI. c) Schematic energy level alignment at the ZnO NPs (pristine unannealed and annealed) and PbS@TBAI interfaces deduced from the UPS data at short-circuit conditions.

.

SVII: EQE spectra analysis of as-prepared PbS QDs solar cells.

As shown in Figure S11, the full-spectrum (350nm-1100nm) external quantum efficiency (EQE) analysis as a function of the ε_{gap} was carried out on the as-prepared PbS QDSCs (ε_{gap} ranges from 1.37 eV to 0.84 eV, the device structure description can be found in the main text). The EQE analysis of a certified Si reference cell and area masks were also applied to ensure the veracity and reliability of the analysis. At lower photon energies, the first exciton absorption peak is clearly visible in the QDSCs such as 1.37 eV, 1.3 eV, and 1.2 eV. Besides of the glass, indium doped tin oxide (ITO), zinc oxide nanoparticle (ZnO) absorption and light reflections, the as-prepared PbS QDSCs exhibit high EQE performance and peaking at photon energy of 3.35 eV to 2.95 eV. Table S1 lists a comparison between J_{sc} values which

are extracted from the solar simulator and the quantum efficiency system. Due to the electrode contact problems and light source fluctuation, there is a slight deviation between these two independent analysis systems. In the best condition, the current density mismatch can be as small as 0.5mA/cm^2. Figure S17 provides another comparison between a 1.37eV PbS QDSC and a CJQDSC which containing layers of 1.03 eV, 1.23 eV and 1.37 eV PbS QDs. The EQE spectra and J-V curves were measured independently with a mask (0.012 cm^2). It can be found that the improvement of solar cell performance between QDSC and CJQDSC can be attributed to the enhanced light absorption and the improved fill factor. The current densities mismatches between these two samples are 0.49 mA/cm^2 and 2.2 mA/cm^2.

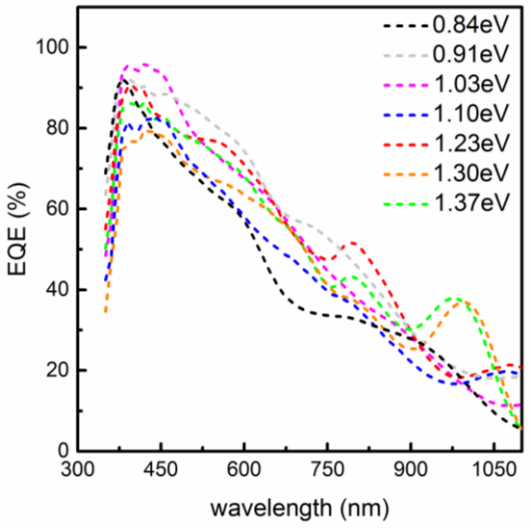

Figure S11 EQE spectra of PbS QDSCs with different ε_{gap}.

Table S1. Comparisons of the current density mismatch between quantum efficiency analysis system and solar simulator system on the as-prepared different ε_{gap} champion QDSCs. The current density of EQE system is integrated under AM1.5G TILT (ASTM-G173-03) with solar cell mask area 0.012 cm^2, EQE of champion devices are quoted in brackets.

Type	ε_{gap}(eV)	J_{sc} (mAcm^{-2})	J_{sc} (EQE)	Mismatch (mAcm^{-2})
QDSC	0.84	24.47	18.08±2.50 (20.59)	3.88
QDSC	0.91	29.63	23.44±3.70 (27.23)	2.4
QDSC	1.03	26.75	21.64±4.12 (25.83)	0.92
QDSC	1.14	25.36	20.59±4.12 (24.81)	0.55
QDSC	1.23	28.86	22.7±7.30 (30)	1.14
QDSC	1.30	26.39	20.81±1.70 (22.50)	3.89

QDSC	1.37	27.52	22.37±3.70 (26.07)	1.45

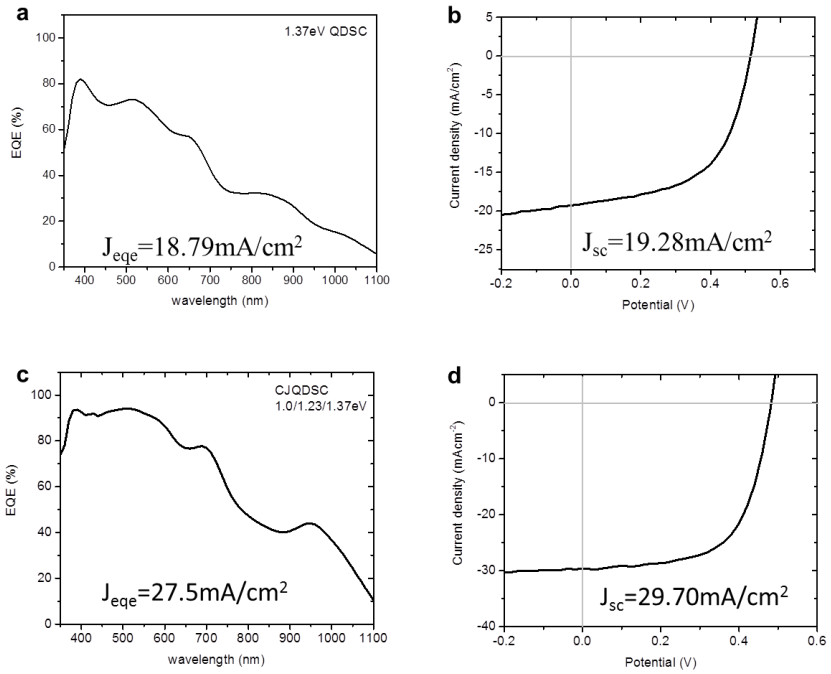

Figure S12. Comparisons of the current density mismatch between quantum efficiency analysis system (a, c) and J-V curves recorded under solar simulator system (b, d) (b,d). The current density from the EQE system is integrated under AM1.5G TILT (ASTM-G173-03) with solar cell mask area 0.012 cm^2.

SVIII: XPS analysis of PbS QDs decorated with OA, EDT, and TBAI.

The composition variations of PbS QDs before and after the ligand exchange process were characterized by the quantized XPS analysis. The film was prepared by spin coating three specific layers of QD on top of ITO slide. As shown in Figure S13, the relative area of Pb4f to S2s is changed with the modification of the QD surface. Table S1 list the detail analysis results of the Pb/S ratio with different ligand functionalization. It can be seen that the TBAI ligand replacement do not bring big changing comparing to the OA decoration. However, in the case of EDT coated PbS QD, the Pb/S ratio exhibits a dramatic band edge changing. This is consistent with the different changing trend as shown in the UPS discussion (Figure 3 in the main text).

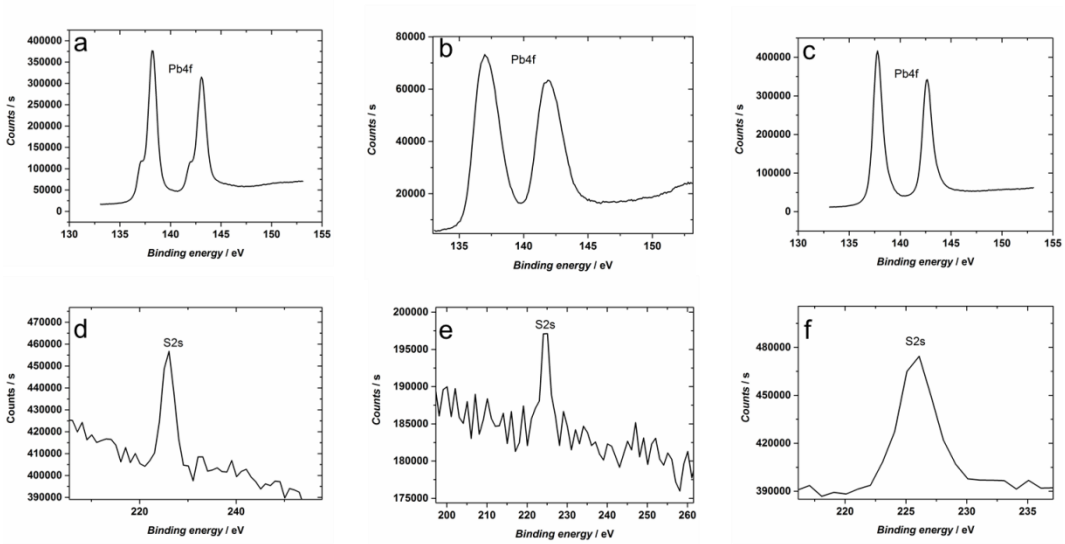

Figure S13 XPS analysis of the as-prepared 1.37 eV PbS QD film on the top of ITO slides. The PbS QDs are ligand exchanged by TBAI (a, d), pristine OA coated (b, e) and ligand-exchanged by EDT (c,f).

Table S2. Quantized XPS analysis results of the atomic ratio between Pb and S.

sample	PbS@OA	PbS@TBAI	PbS@EDT
Pb/S ratio (atomic%)	1.75	1.58	0.85

SIX: Cascaded junctions QDSC (CJQDSC) from assembling 1.03 eV, 1.23 eV and 1.37 eV PbS QDs.

Table S3. Optimized solid-state ligand exchange conditions as a function of QD band gaps.

Band gap (eV)	TBAI (loop/layer)	EDT (loop/layer)
0.84	4	1
0.91	4	1
1.03	2	1
1.14	2	1
1.23	1	1
1.37	1	1

In our optimized preparation condition, different solid-state ligand exchange processes are applied to the different size of QDs which eliminate the difficulties of UPS analysis.[3] As shown in Table S3, due to the different oleic acid loading in the initial stages, ligand washing time has to be adjusted. In Figure S14, the AFM cross-section analysis of PbS QDs films was carried out to control the final thickness of the CJQDSC. As can be seen from Figure S14, the total thickness of reference 1.3 eV PbS QDs solar cell is ca. 320 nm (12 layers 1.3 eV PbS QDs). Figure S15 displays the SEM cross-section image of a CJQDSC which shows the final

film is controlled at ca.334.6 nm. In Figure S16, the absorption spectroscopy analysis was carried out to evaluate the enhancement of light absorption after fabrication of CJQDSC.

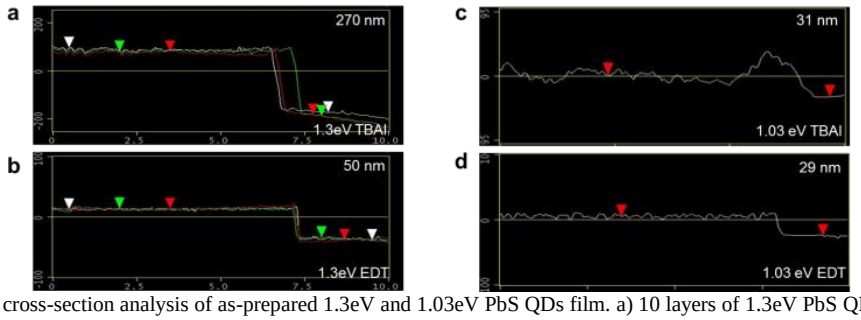

Figure S14. AFM cross-section analysis of as-prepared 1.3eV and 1.03eV PbS QDs film. a) 10 layers of 1.3eV PbS QDs coated with TBAI, and the thickness is measured to be ca. 270nm. b) 2 layers of 1.3eV PbS QDs coated with EDT, and the thickness is measured to be ca. 50nm. c) 1 layer of 1.03 PbS QDs coated with TBAI, and the thickness is measured to be ca. 31nm. d) 1 layer of 1.03eV PbS QDs coated with EDT and the thickness is measured to be 29nm.

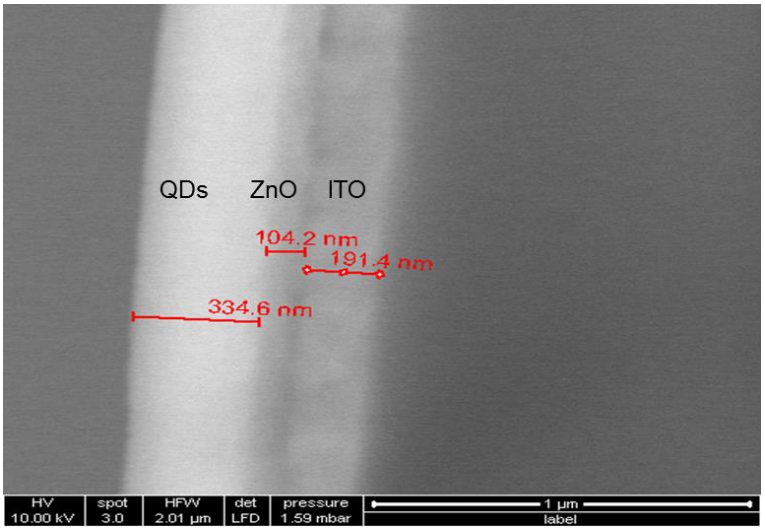

Figure S15. SEM cross-section images of as-prepared CJQDSC (1.03 eV/1.23 eV/1.37 eV). The film contains 12 layers of PbS QDs (1 layer of 1.03 eV and 9 layers of 1.23 eV PbS QDs coated with TBAI; 2 layers of 1.37 eV PbS QDs coated with EDT.) QDs layers total thickness is ca. 334.6 nm, ZnO layers thickness is ca. 104.2 nm and ITO layers thickness is ca. 191.4 nm. Scale bar is 1 µm.

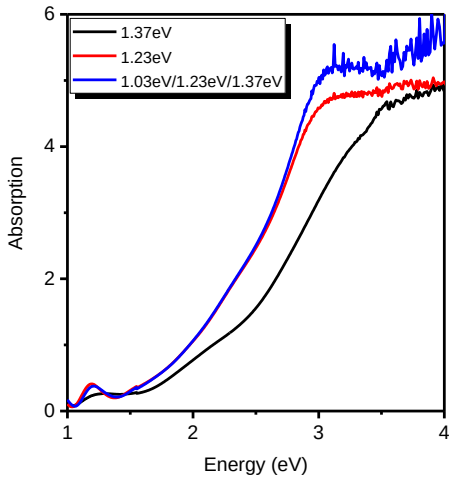

Figure S16. The absorption spectra of QDs films with different band gap. The 1.37 eV and 1.23 eV QDs films consist with 10 layers of TBAI coated QDs and 2 layers of EDT coated QDs. For the CJQDs film, it contains 1 layer of 1.03 eV PbS QDs coated with TBAI, 9 layers of 1.23 eV PbS QDs coated with TBAI and 2 layers of 1.37 eV PbS QDs coated with EDT.

SX: Champion CJQDSC from 1.03 eV /1.23 eV /1.37eV PbS QDs.

In Figure S17, a champion CJQDSC made from the 1.03 eV /1.23 eV /1.37eV PbS QDs has a PCE of 9.05% and shows robust stability. The time-dependent PCE evolution of a CJQDSC during 20 weeks in the ambient storage condition is provided.

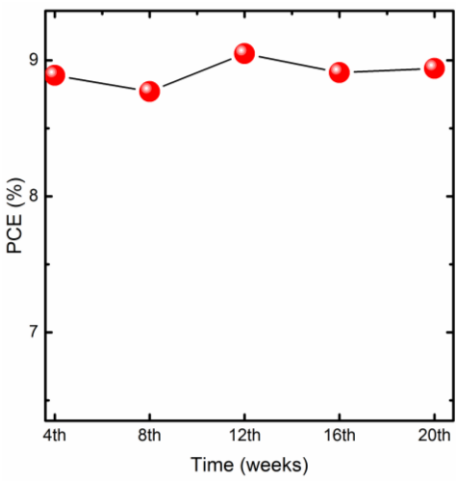

Figure S17. Time-dependent PCE evolution from as-prepared champion PbS CJQDSC. The cell is stored in the ambient air condition.

(1) Zhang, J.; Crisp, R. W.; Gao, J.; Kroupa, D. M.; Beard, M. C.; Luther, J. M. Synthetic Conditions for High-Accuracy Size Control of PbS Quantum Dots. *J. Phys. Chem. Lett.* **2015,** *6*, 1830-1833.
(2) Weidman, M. C.; Beck, M. E.; Hoffman, R. S.; Prins, F.; Tisdale, W. A. Monodisperse, Air-Stable PbS Nanocrystals via Precursor Stoichiometry Control. *ACS Nano* **2014,** *8*, 6363-6371.
(3) Miller, E. M.; Kroupa, D. M.; Zhang, J.; Schulz, P.; Marshall, A. R.; Kahn, A.; Lany, S.; Luther, J. M.; Beard, M. C.; Perkins, C. L., et al. Revisiting the Valence and Conduction Band Size Dependence of PbS Quantum Dot Thin Films. *ACS Nano* **2016,** *10*, 3302-3311.